COMPARISON OF UPWELLING INDICES OFF BAJA CALIFORNIA DERIVED FROM THREE DIFFERENT WIND DATA SOURCES

PAULA PÉREZ-BRUNIUS
Departamento de Oceanografía Física
Centro de Investigación Científica y de Educación Superior de Ensenada
Km 107 Carretera Tijuana-Ensenada
Ensenada, BC 22860
MÉXICO
brunius@cicese.mx

MANUEL LÓPEZ AND ALEJANDRO PARÉS-SIERRA
Departamento de Oceanografía Física
Centro de Investigación Científica y de Educación Superior de Ensenada
Km 107 Carretera Tijuana-Ensenada
Ensenada, BC 22860
MÉXICO

JESÚS PINEDA
Biology Department MS 50
Woods Hole Oceanographic Institution
Woods Hole, Massachusetts 02543
USA

ABSTRACT

We compared the NOAA Southwest Fisheries Science Center's Environmental Research Division (formerly Pacific Fisheries Environmental Laboratory: PFEL) coastal upwelling indices along the northern Baja California coast with those derived from winds measured by coastal meteorological stations and estimated by the QuikSCAT satellite. With the exception of the PFEL series at 33°N, the three data sets compare reasonably well, having similar typical year patterns, correlations >0.6, and significant coherences for periods three to five days or longer. By contrast, the seasonal variations, the timing and magnitude of maximum upwelling, and the variability of the PFEL indices at 33°N are significantly different compared to all the other time series, including QuikSCAT at that location. The performance of the QuikSCAT winds close to shore was evaluated using the coastal meteorological station data. Although large root-mean-square (RMS) errors in direction were found for the QuikSCAT winds, both datasets have properties similar to the variance ellipses, and show reasonable coherences for frequencies in the weather band and lower, particularly south of 33°N.

INTRODUCTION

Winds near the Pacific Coast off Baja California blow predominantly from the north-northwest, causing an offshore Ekman transport that results in year-round upwelling of cold, relatively saline and nutrient-rich waters in the coastal region (Lynn 1967; Bakun and Nelson 1977; Huyer 1983; Schwing et al. 1996; Strub and James 2000). Coastal upwelling helps explain the large productivity along the North American coast and upwelling intensity has been linked with variability in fish stocks and other factors affecting coastal ecosystems (e.g., Reid et al. 1958; Ryther 1969; Longhurst 1998). Researchers have also used upwelling variability to explain zooplankton population spatial processes in coastal systems (Peterson et al. 1979), and more recently a link between latitudinal variability in coastal upwelling and intertidal larval supply, population dynamics, and community structure has been hypothesized (Roughgarden et al. 1988; Connolly et al. 2001).

Coastal Upwelling Indices (CUI) at 15 standard stations along the North American coast have been generated since 1945 by the NOAA Fisheries Southwest Fisheries Science Center's Environmental Research Division (formerly the Pacific Fisheries Environmental Laboratory: PFEL), and are publicly available at its website (http://www.pfel.noaa.gov/). The indices are estimates of the offshore Ekman transport obtained from geostrophic winds, which in turn are derived from the surface pressure fields of the operational atmospheric model provided by the U.S. Navy Fleet Numerical Meteorology and Oceanography Center (FNMOC), Monterey, California. For historic reasons, and to be consistent with previous references, we will refer to the Environmental Research Division coastal upwelling indices as the "PFEL indices."

The PFEL indices have been widely accepted, with more than 50 regular users each month, several dozens of additional requests for the data each year, and more than 400 scientific publications referencing them (Schwing et al. 1996). The studies cover topics ranging from descriptions of coastal circulation patterns, climate change, and linkages between environmental and biological variability. They have been particularly popular in linking physical forcing with marine population variability (e.g., Ainley et al. 1993; Parrish and Mallicoate 1995; Rau et al. 2001; Koslow et al. 2002; Ladah and Zertuche 2004).

The limitations of the PFEL indices have been discussed elsewhere (e.g., Schwing et al. 1996). The most important may be the fact that upwelling is the combined effect of two processes: the offshore Ekman transport due to the alongshore component of the winds (which is what the PFEL indices represent) and the Ekman pumping that results from the curl of the winds

near the coast. The latter may be an equally or even more important contributor to surface Ekman divergence and upwelling, especially downstream of islands, capes, and other coastal promontories (Bakun and Nelson 1991; Enriquez and Friehe 1995; Schwing et al. 1996; Münchow 2000; Pickett and Paduan 2003; Koracin et al. 2004; Pickett and Schwing 2006).

PFEL indices off California have been compared with the offshore Ekman transport derived from satellite winds close to the PFEL indices grid points (Pickett and Schwing 2006), and the offshore Ekman transport and Ekman pumping close to shore using the 9 km resolution Coupled Ocean/Atmospheric Mesoscale Prediction System (COAMPS) model (Pickett and Paduan 2003; Pickett and Schwing 2006). Pickett and Schwing (2006) found reasonable agreement between weekly averages of the PFEL indices and the corresponding offshore Ekman transport derived from satellite winds on the PFEL grid, although a better comparison was found using the model winds (instead of the geostrophic winds used for the PFEL indices). On the other hand, the high resolution model showed narrow bands (about 20 km offshore by 50 km alongshore) of strong wind stress and wind stress curl adjacent to major coastal promontories, suggesting that Ekman pumping may be as large a contributor to upwelling as offshore Ekman transport. Nevertheless, Pickett and Paduan (2003) found a significant correlation, similar means, and seasonal variations between the PFEL indices and the net upwelling (offshore Ekman transport plus Ekman pumping), in spite of the fact that the PFEL indices do not include Ekman pumping. They attribute this similarity to an overestimation of the offshore Ekman transport by the PFEL indices, given that the winds generally increase with offshore distance, resulting in stronger winds at the PFEL grid than in the coastal zone.

These studies conclude that the PFEL indices are reasonable estimates of the regional upwelling off North America, but higher spatial resolution models are needed to accurately represent the magnitude and variability of local coastal upwelling.

Finally, intertidal ecologists have used PFEL indices to explain temporal and latitudinal variation in invertebrate recruitment. This usage is problematic because PFEL indices do not accurately represent nearshore hydrodynamics where invertebrate larvae are most likely to be found; PFEL indices are unlikely to capture the small-scale flows and the vertical variability that transport larvae and influence larval distribution. Moreover, the usage is also problematic because settled individuals suffer large mortalities which are time- and space-dependent, and these post-settlement mortalities are disregarded when linking PFEL indices with recruitment.

In this study we focus only on the offshore Ekman transport component of coastal upwelling, although the spatial variability of the winds and their effect on the offshore Ekman transport estimates will be discussed. We compare the daily PFEL indices with the average daily offshore Ekman transport from wind data measured both by coastal meteorological stations and satellites for the northern Baja California region. The objective is to evaluate the differences between the three different estimates, and discuss how representative they are of the coastal upwelling in the region between La Jolla, California, and Punta Eugenia, Baja California. In addition, the performance of satellite winds near the coast is evaluated using the coastal meteorological stations data.

DATA AND METHODS

The Coastal Upwelling Index (CUI) has been defined as the cross-shore Ekman transport per 100 m coastline, positive for offshore transport, i.e., upwelling conditions. Its units are m^3/s per 100 m coastline (Bakun 1975):

$$CUI = \frac{\tau}{\rho f} \times 100 \qquad (1)$$

where $\rho = 1025$ kg/m^3 is the mean density of the upper water layer, f- the Coriolis parameter, and τ is the alongshore wind stress (defined positive when directed towards the equator) estimated as in Bakun and Nelson (1977):

$$\tau = \rho_a C_d U_{10} || U_{10} || \qquad (2)$$

here $\rho_a = 1.22$ kg/m^3 is the density of air; C_d is the drag coefficient, which for the PFEL historical 3° upwelling index has been used as a constant ($C_d = 0.0013$); and U_{10} is the alongshore wind speed at 10 m (positive towards the equator).

Daily coastal upwelling indices were estimated from three different data sources: winds measured directly by coastal meteorological stations, winds estimated from scatterometer satellite data, and geostrophic winds calculated from an atmospheric operational model. The study period was from 30 August 2000 through 16 March 2004.

Pacific Fisheries Environmental Laboratory indices

The daily Coastal Upwelling Indices provided by the NOAA Southwest Fisheries Science Center's Environmental Research Division (formerly the Pacific Fisheries Environmental Laboratory [PFEL]) were used for this study. The indices result from the geostrophic winds derived from six-hourly synoptic surface atmospheric pressure fields. The pressure fields were provided on a global spherical 1° mesh by the U.S. Navy Fleet Numerical

TABLE 1
Meteorological stations information

Station name	Position of sensor (lat, lon, height)	Angle with coast (relative to east)	Angle of maximum variance (relative to east)
La Jolla	32.9°N, 117.3°W 20m	–39° (–65°)	–62°
Punta Banda	31.7°N, 116.7°W 20m	–60°	–69°
Punta Baja	29.9°N, 115.8°W 19m	–65° (–51°)	–55°
Morro Santo Domingo	28.2°N, 114.1°W 56m	–41°	–34°

Location of the meteorological stations (latitude, longitude, and height above sea level). The angle with the coast is used to estimate alongshore wind stress. In La Jolla and Punta Baja, those angles are the ones used for the PFEL indices at those latitudes; the angles derived from a linear fit to the coastline 0.5° north and south of those stations are in parenthesis.

Meteorological and Oceanographic Center (FNMOC), Monterey, California. The historical daily indices were derived from a 3° mesh that was interpolated from the daily averages of the wind-driven cross-shore transports obtained from the six-hourly FNMOC 1° pressure fields (http://www.pfel.noaa.gov). We used the CUI values at 33°N, 119°W; 30°N, 119°W; and 27°N, 116°W (fig. 1). These locations are 110 km, 275 km, and 130 km from shore, respectively (Pickett and Schwing 2006). The angles (rel. to east) used to obtain the along-shore component of the wind were −39°, −65°, and −63°, respectively (Bakun 1975). We will refer to these time series as the PFEL indices.

Meteorological stations

Winds were sampled at four coastal meteorological stations and averaged every hour (tab. 1, fig. 1). The meteorological stations were set in well-exposed locations, on top of lighthouses at capes and points along the coast. The La Jolla data came from the meteorological station located on the Scripps Oceanographic Institution pier. We obtained the alongshore component of the wind using the angles shown in Table 1. At Punta Banda, the angle was obtained by making a linear fit to the coastline 0.5° north and south of the station, while at Morro Santo Domingo the mean angle of the coastline between Punta Baja and the meteorological station in question was used. We used the same angles for La Jolla and Punta Baja as the corresponding angles used for the PFEL indices at those latitudes. A linear fit to the local coastline gives a different angle than the angles used by the Bakun indices, especially off La Jolla (tab. 1). This is the case given that the PFEL indices use the mean direction of the coastline within the 3° box containing the grid point, and the coastline north of San Diego has a strong change of direction towards the northwest north of 33°N, while it has more of a north-south orientation to the south. At the four stations, the axes of maximum variance of the winds were closely aligned with the direction of the coast, more so than with the angle used by PFEL.

The daily upwelling indices result from daily averages of the indices calculated from the hourly alongshore wind stress. In this report, the time series of upwelling

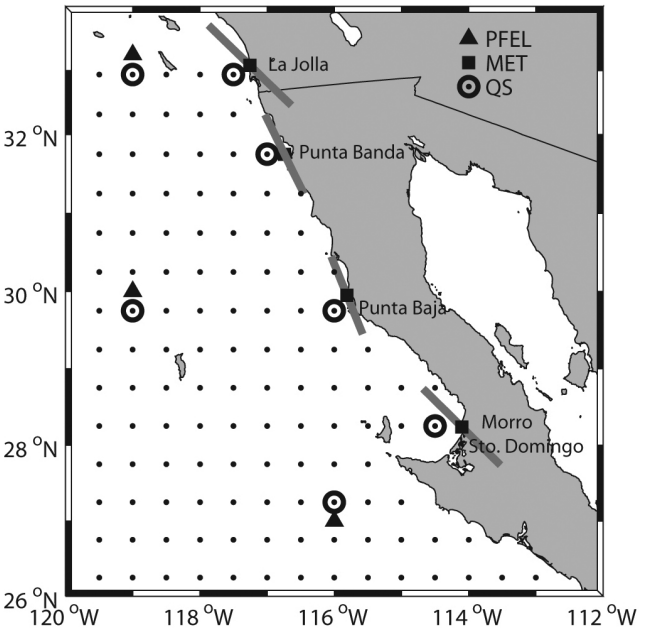

Figure 1. Position of the PFEL grid points (triangles), meteorological stations (squares), and QuikSCAT grid (dots). The open circles denote the QuikSCAT grid points closest to the PFEL and coastal meteorological stations. The dark gray lines at the coastal stations show the angle of the coastline used to obtain the alongshore component of the wind. At 33°N and 30°N, the angles are the ones used for the calculation of the PFEL indices.

indices derived from the meteorological station data is called MET. In addition, a time series of daily wind averages was produced to compare with the QuikSCAT satellite-derived winds.

QuikSCAT winds

We use gridded and interpolated QuikSCAT Level 3 data (0.5° × 0.5° and 12 hour resolution) provided by the Jet Propulsion Laboratory Air-Sea Interaction & Climate Team (http://airsea.jpl.nasa.gov/DATA/QUIKSCAT/wind/). The accuracy of the measurement is 2 m/s in magnitude and 20° in direction for speeds larger than 3 m/s.

Near the coast, land contamination and other technical difficulties restrict scatterometer data to within a few tens of kilometers from land. Data analysis has shown that QuickSCAT vector wind measurements are accu-

rate within approximately 25–30 kilometers of the coastline (Tang et al. 2004). Tang et al. (2004) argue that this increase in error near the coast is likely because the geophysical model function is inadequate and the removal scheme in addressing coastal conditions and light wind situations is ambiguous. In addition to the technical difficulties in determining winds near the coast, the increase in small-scale time and space variations associated with land (e.g., sea-land breezes, topographically induced variations) can be smoothed by the satellite space-averaging process and aliased by the twice-daily sampling that compounds the problem (e.g., Pickett et al. 2003). In fact, standard QuikSCAT products are the result of across-track sweeps averaged in 25 × 25 km wind vector cells, and the outputs are not used if any part of the fields of view is contaminated by land.

Time series of QuikSCAT winds were obtained for the grid points closest to the PFEL and MET locations (see fig. 1). Upwelling indices for the 12 hourly winds were derived with equation 1, using the angles for the alongshore component that correspond to the PFEL and MET series, and averaged to produce daily time series (which we refer to as QS). Daily means of each wind component were also produced, to compare with meteorological stations' winds. The PFEL stations are 150 to 280 km from the coast, while the MET stations are on the coast. We refer to the PFEL and corresponding QS points as the "offshore stations," while the MET and corresponding QS points will be called "coastal stations." Separation between the shore and QS coastal stations are: 26 km at San Diego, 25 km at Punta Banda, 29 km at Punta Baja, and 39 km at Morro Santo Domingo, all of these near to the accuracy limit of satellite winds close to land. Hence, we compared them with the corresponding meteorological station data to see how well they reproduce the coastal winds off Baja California.

Finally, we also derived upwelling indices for the entire QuikSCAT grid within the region of interest, using the angles shown in Figure 2, to obtain the alongshore component of the wind.

Coherences

Coherences were estimated to compare the datasets on the frequency domain. The time series were divided into 20 segments, each smoothed with a Hanning window. The coherences were estimated for each window, using the periodogram method to calculate the corresponding spectral power densities. The final coherence is the ensemble average over all segments, with 20 equivalent degrees of freedom, and a frequency resolution of 0.015 cpd (Emery and Thomson 2001).

To make sure that the above coherences did not depend on the time period sampled, the series were divided in four segments of 323 days each, and the coherences for each segment were calculated with the method described above (20 equivalent degrees of freedom and a frequency resolution of 0.063 cpd). The mean of the coherences for the four segments represented the coherence for the entire time series in most cases. Both estimates are in the results for comparison. Please note that by "coherence" we mean the "squared coherence" or "coherence spectrum" (Julian 1975; Emery and Thomson 2001).

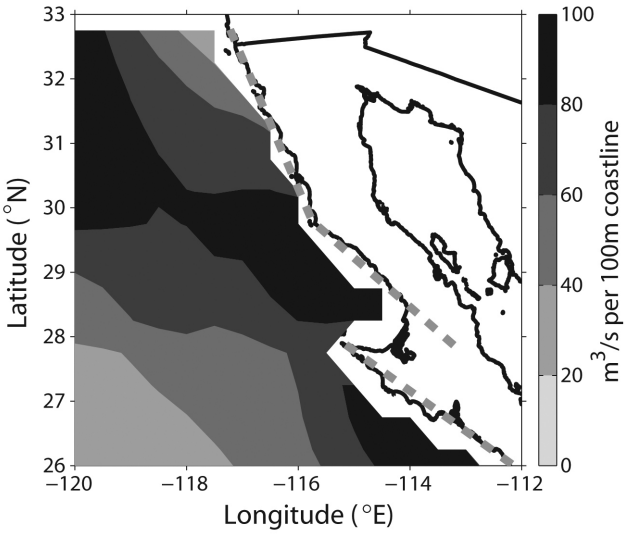

Figure 2. Mean offshore Ekman transport calculated from the QuikSCAT gridded field, using the dotted gray lines as the direction of the coastline.

We also calculated the clockwise and counterclockwise rotary spectral components for the QuikSCAT coastal and meteorological station winds. To determine how similar the circularly polarized rotary components of the two vector series were, the inner-coherence (between the co-rotating components) and outer-coherence (between the counter-rotating components) were obtained (Emery and Thomson 2001).

RESULTS

Coastal Upwelling Indices

Spatial pattern from QuikSCAT The mean of the indices calculated with the QuikSCAT winds shows the spatial variations in the coastal upwelling estimates that result from the large-scale shear of the wind (fig. 2). Although the QuikSCAT grid may not resolve effects on the shear of the wind due to islands, headlands, capes, and friction with coastal topography, it is clear that the large-scale spatial pattern shows variations on the magnitude of the upwelling indices both along the coast and with distance from shore. Off La Jolla, the indices increase steadily away from the shore. The offshore maximum observed at that latitude is a consequence of the strong jet that separates from the coast at Point

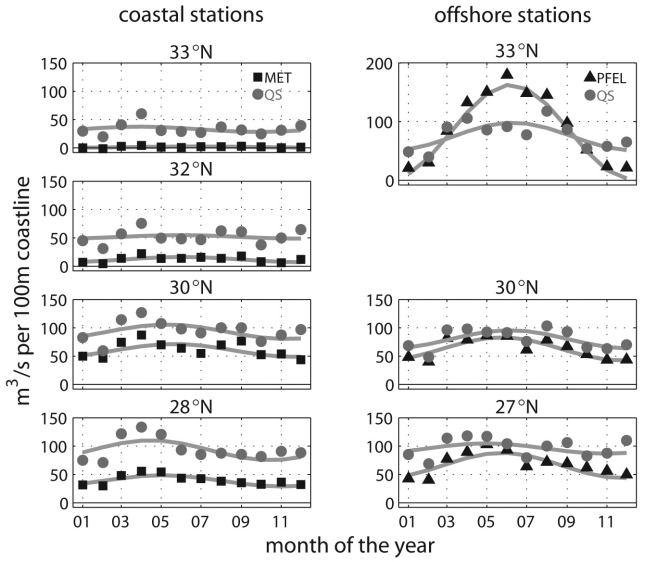

Figure 3. Typical year for the coastal upwelling indices. Each point represents the 3-year mean (2001–03) of the monthly averages. The light gray lines show the corresponding annual fit. Left panels: meteorological stations (squares) and coastal QuikSCAT stations (circles). Right panels: PFEL (triangles) and offshore QuikSCAT stations (circles).

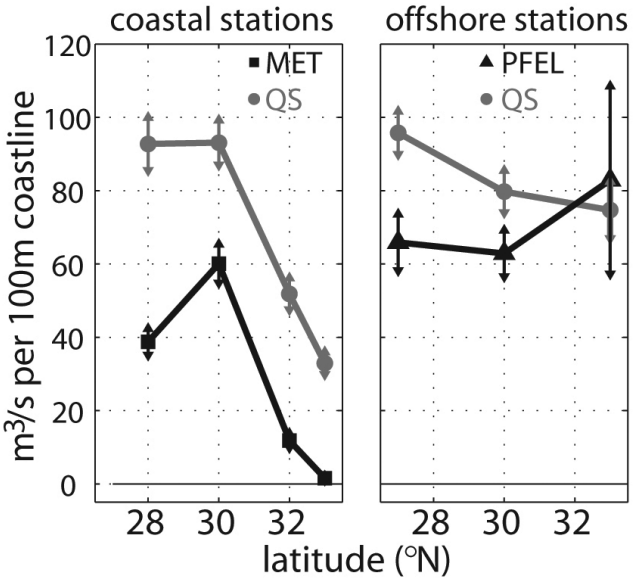

Figure 4. Mean upwelling indices with corresponding 95% interval for the coastal (left panel) and offshore stations (right panel). Meteorological stations (squares), PFEL (triangles), and QuikSCAT estimates (circles).

Conception (~34.5°N), caused by the 90° turn of the coastline (Winant and Dorman 1997; Münchow 2000). From Punta Baja southwards, the pattern reverses, with the largest indices found near the shore. This spatial pattern is maintained throughout the year, only varying in magnitude.

Typical year and basic statistics Monthly means were obtained and averaged over the three complete years of the time series. Figure 3 shows the resulting typical year for the offshore and coastal stations, including the annual cycle fit obtained with harmonic analysis. The mean for the entire length of the time series with a 95% confidence interval is plotted in Figure 4. For the coastal stations, the typical year for the MET and QS series follow the same general pattern; maximum values in April, a secondary maximum in August-September (in most cases), and minimum values in February. A third maxima in December is usually found in the QuikSCAT series. The annual cycle fit explains less than 50% of the variance, except at the southernmost meteorological station, where the fit is better because the series has less of a bimodal character (the late summer maxima is small). Finally, the QS values are larger than the corresponding MET values by a near constant offset of 30–60 m^3/s per 100 m coastline (fig. 4). Note that the indices tend to get smaller towards the north, with minimum values at 33°N (figs. 3 and 4). The highest values are observed at 30°N, although QS shows no major difference between Punta Baja (30°N) and Punta Eugenia (28°N).

For the offshore stations, QS also shows maximum values in April and August-September. The difference with the coastal stations is that both maxima have similar magnitudes. By contrast, the PFEL series show the first maxima later, especially off La Jolla (33°N) where the indices peak in June. That particular PFEL series stands out from the rest, with a strong annual cycle (explaining 98% of the variance), and the largest upwelling index values of all (larger than 150 m^3/s per 100 m coastline in June). At this location, the monthly PFEL indices generally exceed the QS values, with a mean offset of 10 m^3/s. By contrast, the QS indices have slightly larger values than the corresponding PFEL values at the two southern stations (mean offset of 20–30 m^3/s per 100 m coastline, figs. 3 and 4). While a decline towards the north is suggested by the MET series and by the QS indices both offshore and near the coast, the PFEL indices suggest that the strongest upwelling of the entire region occurs in the summer at 33°N. The large variability for PFEL at that station also stands out as anomalous compared to the results from the other stations and datasets.

Correlations and coherences Figures 5 and 6 show the correlation and coherences for time series of offshore PFEL versus QS stations, and the coastal MET versus QS stations. The lowest correlations are found at 33°N (0.60 offshore, 0.45 coastal), and the highest at 30°N (around 0.70 both offshore and coastal). QuikSCAT shows better correlations offshore with the PFEL time series than with MET at the coastal stations.

The coherences (fig. 6) are generally significant for frequencies smaller than 0.2–0.3 cpd (periods larger than 3–5 days), and the series vary nearly in phase for those

TABLE 2
Basic statistics for the daily upwelling indices

Station name	Database	Mean	Standard deviation	Variance explained by annual cycle
Coastal Stations				
La Jolla (33°N)	MET	2.0 ± 0.6	7.0 ± 0.4	20%
	QS	33 ± 3	29 ± 2	11%
Punta Banda (32°N)	MET	12 ± 2	20 ± 1	43%
	QS	52 ± 4	38 ± 3	3%
Punta Baja (30°N)	MET	60 ± 5	44 ± 4	37%
	QS	93 ± 6	54 ± 5	28%
Morro Sto. Dom. (28°N)	MET	39 ± 4	25 ± 3	67%
	QS	93 ± 7	51 ± 5	43%
Offshore Stations				
La Jolla (33°N)	PFEL	83 ± 26	89 ± 21	98%
	QS	75 ± 8	58 ± 6	53%
Punta Baja (30°N)	PFEL	63 ± 6	53 ± 5	72%
	QS	80 ± 6	52 ± 4	46%
Punta Eugenia (27°N)	PFEL	66 ± 8	45 ± 6	67%
	QS	96 ± 6	54 ± 4	17%

The mean and standard deviations are shown with the 95% confidence interval. Units are in m^3/s per 100 m coastline. The percentage of variance explained by the annual fit corresponds to the ratio of the variance of the typical year to the variance of the annual fit. PFEL–NOAA Southwest Fisheries Science Center's Environmental Research Division (formerly Pacific Fisheries Environmental Laboratory) coastal upwelling indices; MET–upwelling indices derived from the coastal meteorological stations' wind data; QS—upwelling indices derived from QuikSCAT winds close to the PFEL locations (offshore) and the meteorological stations (coastal).

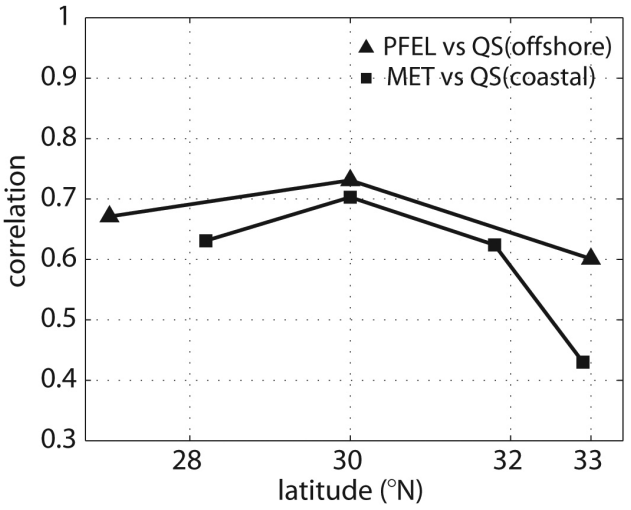

Figure 5. Correlations between PFEL and offshore QuikSCAT upwelling indices (triangles), and meteorological stations versus coastal QuikSCAT upwelling indices (squares).

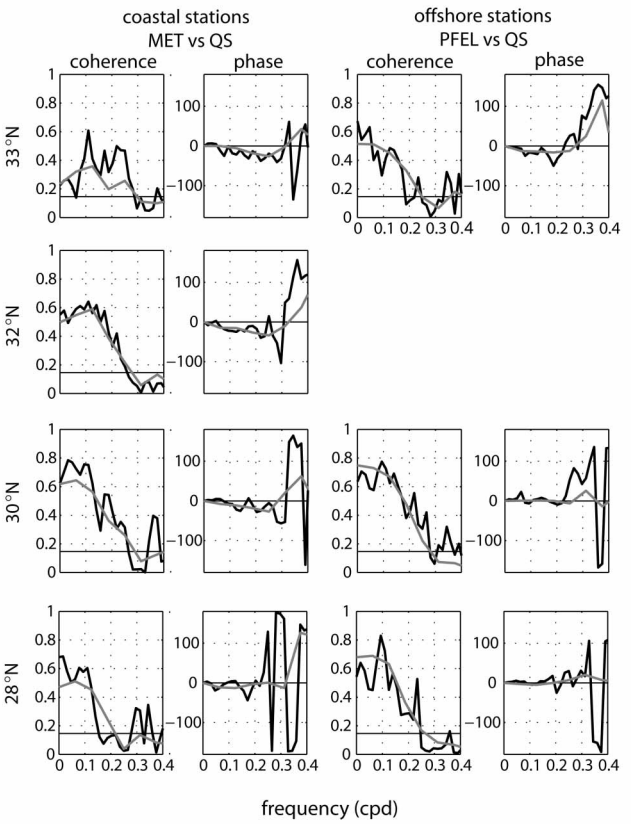

Figure 6. Point-by-point coherences and phases (in degrees) of the upwelling indices. The thick black lines show the calculation over the entire length of the time series, while the light gray lines show the average over the coherences and phases for each 323-day segment. The coherences were calculated using the averaged periodogram method with 20 degrees of freedom (see text for more details). Left panels: meteorological versus QuikSCAT coastal stations. Right panels: PFEL and QuikSCAT offshore stations. Positive phases indicate that the QuikSCAT series leads for both the left and right panels.

frequencies, with lags mostly shorter than two days (phases <40°). The lowest coherences both offshore and at the coastal stations are found at 33°N (values less or equal to 0.6), while at the rest of the stations the values are generally larger than 0.5.

Coastal versus offshore To compare the offshore versus the coastal estimates of the upwelling indices, we calculated the mean difference, correlations, and coherences between the PFEL and the corresponding MET time series, and between the offshore and coastal QS time series (figs. 7 and 8). The comparison between the QS series provides information about the differences in the estimates due to the large-scale shear of the winds (i.e.,

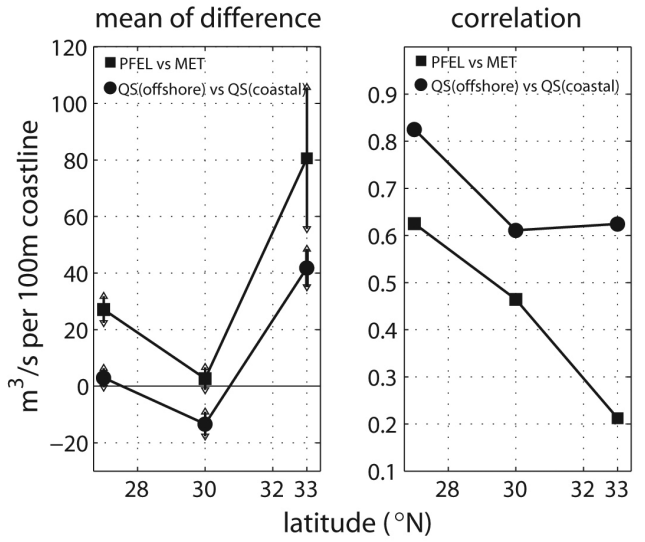

Figure 7. Comparisons between the offshore and coastal estimates of the upwelling indices. Left panel: mean of the difference between the PFEL and meteorological time series (squares, positive for PFEL > MET) and offshore minus coastal QuikSCAT series (circles), with corresponding 95% confidence interval. Right panel: correlations between the PFEL and meteorological time series (squares), and between the offshore and coastal QuikSCAT time series (squares).

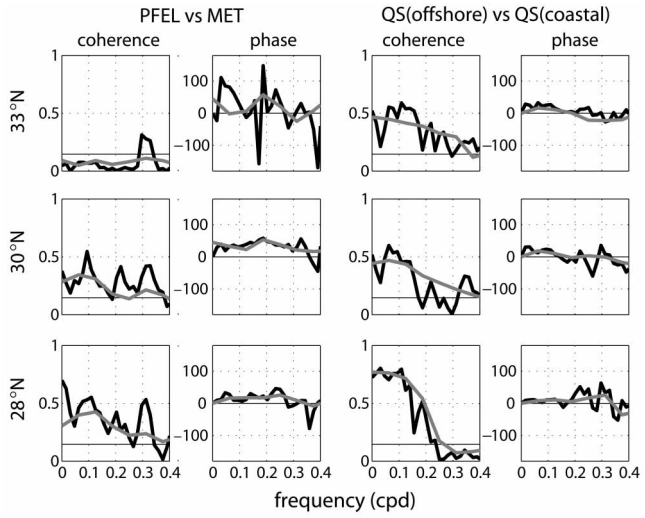

Figure 8. Coherences and phases between the offshore and coastal stations upwelling time series. The thick black lines show the calculation over the entire length of the time series, while the light gray lines show the average over the coherences and phases for each 323 day segment. The coherences were calculated using the averaged periodogram method with 20 degrees of freedom (see text for more details). Left panels: PFEL versus meteorological stations. Right panels: QuikSCAT offshore versus coastal stations. Positive phases indicate that the coastal stations lead the offshore stations.

variations in the winds with distance from shore), while the comparison of the PFEL and MET indices provides information about the difference in estimates due to both the large-scale shear of the wind and differences between the two data sources.

At 33°N the indices calculated on the offshore station render a much larger value than the coastal station, the

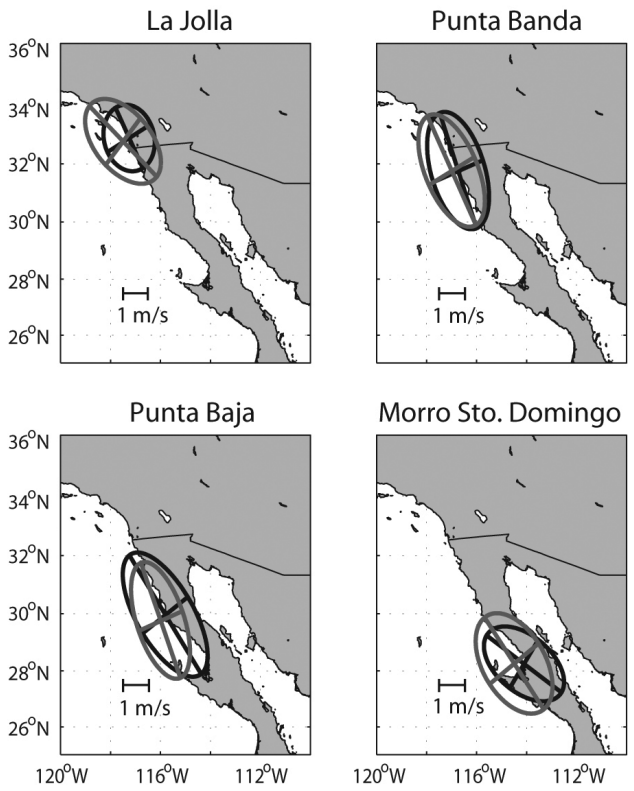

Figure 9. Ellipses showing the orientation of the principal axes and standard deviation along principal axes for the meteorological (black) and coastal QuikSCAT (gray) stations winds.

QS stations (40 unit bias), and the PFEL and MET stations (80 unit bias). For other latitudes, the differences are less than 30 m^3/s (per 100 m of coastline), in some cases not significantly different than zero (QS at 28°N), including a 15 m^3/s (per 100 m of coastline) larger mean value at the coast than offshore for QS at 30°N. Correlations are higher between the QS offshore and coastal stations (>0.6) than between the PFEL and MET stations (<= 0.6). The higher correlations for both comparisons are observed in the southernmost station (fig. 7).

Coherences between PFEL and MET at 30° and 28°N are generally significant for frequencies less than 0.3 cpd, while at 33°N they are nearly zero (fig. 8). QS shows significant coherences at the three latitudes, but mostly for frequencies less than 0.2 cpd. In both comparisons, higher coherences are found at the southernmost station (fig. 8). For the frequencies where the coherence is significant, the series vary more-or-less simultaneously (lags less than two days, which correspond to phases <40°).

QuikSCAT versus meteorological station winds

To see how well the coastal QS winds represent those measured by the meteorological stations, the variance ellipses for both time series were calculated (fig. 9). Except for the northernmost station, the eccentricity

TABLE 3
RMS errors for the QuikSCAT coastal stations

	La Jolla (33°N)	Punta Banda (32°N)	Punta Baja (30°N)	Morro Sto. Domingo (28°N)
Direction (degrees)	109	91	34	36
Magnitude (m/s)	3.1	3.1	2.1	2.8

Root-mean-square differences between the QuikSCAT winds at the coastal stations and the winds measured by the coastal meteorological stations. Accuracy of QuikSCAT winds is 2m/s in magnitude and 20° in direction.

and magnitude of the ellipses' axes are similar, and correlations are larger than 0.6 for the winds along the major axis (figs. 9, 10A, E, and F). Off La Jolla (33°N), the variability along the major and minor axes is pretty much equal for the winds measured by the meteorological station, while the QS winds show larger variability in the alongshore direction. At this station, the correlation along the major axis drops below 0.4 (figs. 10A, C, E, and F).

The mean of the QS winds along the major axis of variance is 2–4 m/s larger than for the MET winds (fig. 10D). The angles of the major axis differ by 7° to 21° at all stations, with the MET winds generally more aligned with the local direction of the coastline (fig. 10B). Table 3 shows the root-mean-square (RMS) differences between the two datasets, where it is clear that the direction of the wind at the coast is badly represented by the QS dataset at 32°N and 33°N, mainly due to larger variability in direction for the MET winds.

The inner-coherences that result from the co-rotating components of the vector series are shown in Figure 11. They are significant for frequencies less than 0.2 cpd, with values larger than 0.5 south of Punta Banda (32°N), particularly for the clockwise components (negative phase). Phase lags are generally less than two days ($|\text{phase}| < 40°$). Figure 12 shows the outer-coherence (which measures the stability between the ellipse orientations of the two vector series for each frequency band: Gonella 1972; Mooers 1973), and the absolute mean difference in orientation of the ellipses. Significant outer-coherences are found for frequencies less than 0.2 cpd for all locations with the exception of 33°N, although the outer-coherence is barely significant for the southernmost station. The mean difference in orientation of the ellipses is generally less than 30°, with smaller and less variable differences at 28° and 32°N.

DISCUSSION AND CONCLUSIONS

The satellite data show the position of maximum alongshore winds to be more than 100 km from the coast off La Jolla, getting progressively closer to shore towards the south, and resulting in maximum winds within 50 km from the coast south of Punta Baja (fig. 2). This pattern of strong northwesterly winds downstream of Point Conception (the point at which the northwesterly oriented central California coastline makes a sharp 90° turn to the east: ~34.5°N), and weak winds near the eastward coast of the Southern California Bight, has been observed in previous studies (e.g., Bakun and Nelson 1991; Winant and Dorman 1997; Münchow 2000; Pickett and Paduan 2003; Capet et al. 2004; Koracin et al. 2004; Pickett and Schwing 2006).

Midway down the Baja California peninsula, the wind profile seems closer to that observed off the Northern California coast by aircraft measurements (Beardsley et al. 1987; Enriquez and Friehe 1995) and high resolution atmospheric models (Koracin et al. 2004), where upwelling-favorable wind maxima were observed 20 km from shore. The northern California nearshore jet seems to be the consequence of a sharp narrowing towards the shore of a shallow marine boundary layer (Beardsley et al. 1987), and tends to behave as a supercritical channel flow. As a result, changes in direction of the coastline result in expansion fans with corresponding acceleration of the northerly winds downstream of Point Arena (Winant et al. 1988).

Winant et al. (1988) point out that the principal requirements for supercritical flow are (1) a shallow marine layer capped by a strong inversion, (2) coastal mountain ranges higher than the marine boundary layer, and (3) wind speeds close to the shallow-water wave speed. They also refer to some early studies that suggest the presence of a thin marine layer along the coastal region of Baja California. Although our data cannot verify this hypothesis, the presence in the spring and summer of a layer of dense fog, capped by a sharp boundary which separates it from the clear skies above, suggests a sharp-and-shallow temperature inversion, which can persist until late in the day. The fog is usually trapped by the coastal mountain ranges, which can reach heights over 600 m. In addition, the meteorological station at Punta Baja recorded mean wind speeds of 5 m/s, with most of the hourly winds falling in the 4–8 m/s window. These values correspond to the shallow wave speed for a layer 100–300 m thick, assuming a value of 0.3 m/s^2 for the reduced gravity as in Winant et al. (1988), so supercritical flow conditions seem likely. If this were the case, the supercritical conditions in combination with the change in the coastline direction may explain the nearshore wind stress maximum observed downstream of Punta Baja by satellite (figs. 2 and 3), coastal meteo-

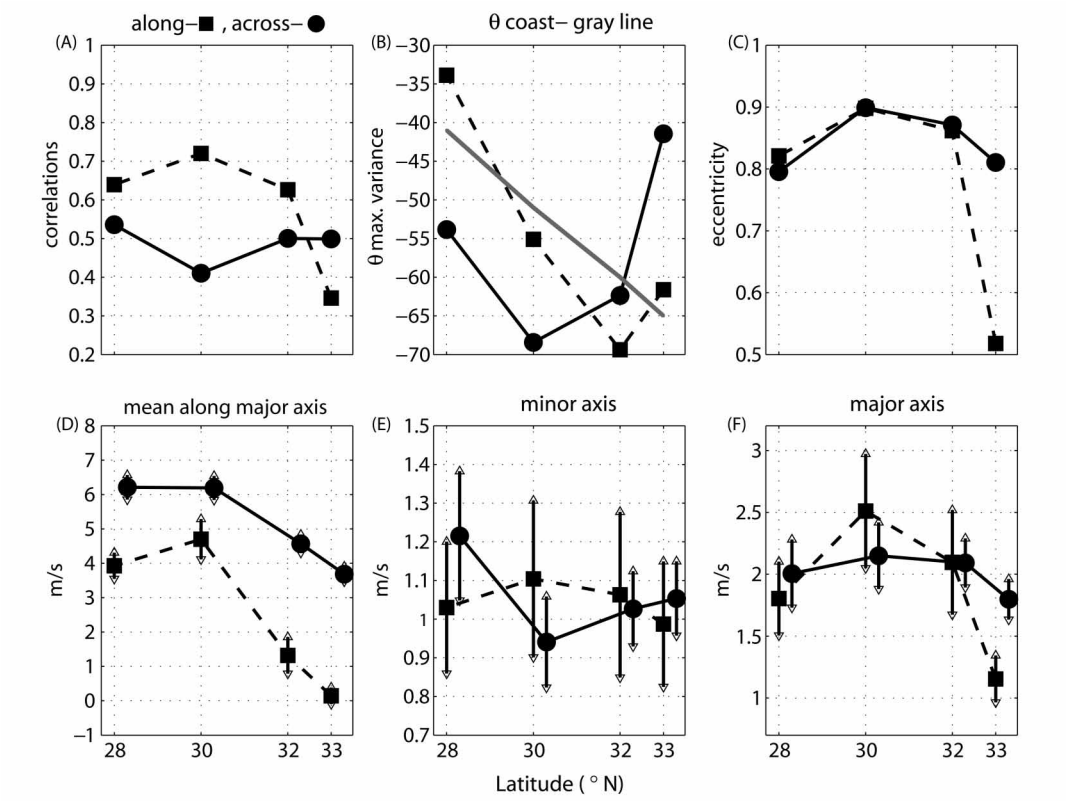

Figure 10. Comparisons between the meteorological and coastal QuikSCAT station winds. Except in (A), circles denote QuikSCAT winds while squares correspond to the meteorological stations winds. (A) correlations along the major (squares) and minor (circles) axis of the wind variance ellipses, (B) angle of maximum variance (relative to the east, the gray line shows the local direction of the coast), (C) eccentricity of the variance ellipses, (D) mean and 95% confidence interval along the direction of maximum variance, (E) and (F) magnitude and 95% confidence interval of the minor and major axis, respectively.

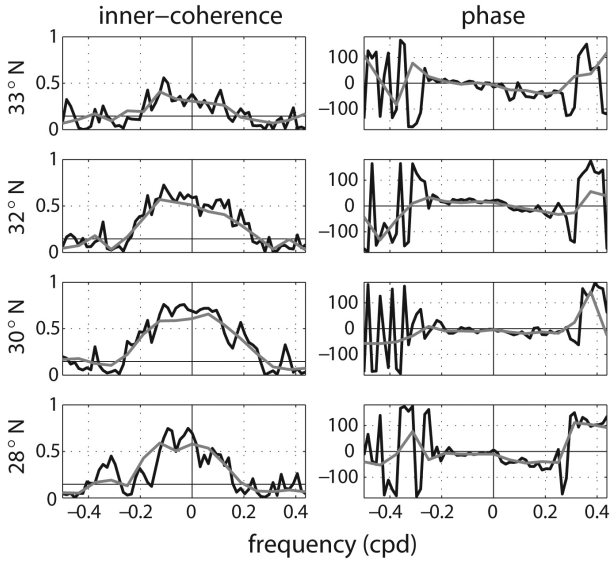

Figure 11. Inner-coherence and phase between the meteorological and QuikSCAT station winds. Negative (positive) frequencies correspond to the coherences of the counterclockwise (clockwise) rotary spectra. The 95% confidence limit is shown as a thin horizontal line. Positive phases mean the winds from the meteorological stations lead the QuikSCAT winds. The thick black lines show the calculation over the entire length of the time series, while the light gray lines show the average over the coherences and phases for each 323 day segment. The coherences were calculated using the averaged periodogram method with 20 degrees of freedom (see text for more details).

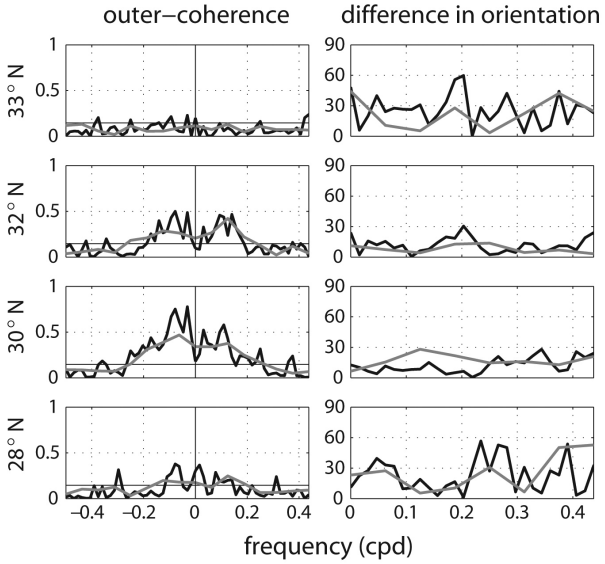

Figure 12. Left panels: outer-coherence between the meteorological and QuikSCAT station winds. Negative (positive) frequencies correspond to the coherences between the counterclockwise rotary spectra of the meteorological stations winds (QuikSCAT winds) and the clockwise rotary spectra of the QuikSCAT winds (meteorological stations data). The 95% confidence limit is shown as a thin horizontal line. Right panels: mean absolute difference in ellipse orientation (in degrees) between the meteorological and QuikSCAT stations winds. The thick black lines show the calculation over the entire length of the time series, while the light gray lines show the average over the calculations for each 323 day segment (see text for more details).

rological stations (figs. 3 and 4), historical ship reports (Nelson 1977; Bakun and Nelson 1977), and high resolution model winds (Koracin et al. 2004). This remains to be tested.

Similarly, the strong northwesterly winds downstream of Point Conception seem to result from separation of the supercritical flow due to the sharp change in the coastline orientation (Winant and Dorman 1997; Münchow 2000; Koracin et al. 2004).

The comparison of the offshore Ekman transports calculated from the coastal QuikSCAT stations and meteorological station winds is almost the same as the comparison between the PFEL and offshore QuikSCAT indices. This is a bit surprising, given that both the PFEL and QuikSCAT upwelling estimates are derived from smooth gridded fields, while the meteorological stations are point measurements. Also, land effects such as the sea breeze and small changes in local topography introduce additional variability to the local coastal winds not present a few kilometers offshore. Finally, satellite winds tend to have large errors near the land boundaries, especially in direction (Pickett et al. 2003). This is reflected in the large RMS errors found between the QuikSCAT and meteorological station winds, which for the northernmost stations were up to five times larger than the accuracy in wind direction of the satellite measurements (20°). Nevertheless, at the stations south of 33°N the variance ellipses have the same eccentricity, their orientation differing by at most 20°, the winds along the major axes correlate reasonably well (correlations >0.6) and, for periods larger than five days, the inner-coherences have values ≥0.5, the outer-coherences are generally significant, and the difference in orientation of the ellipses for each frequency band remained generally below 30°.

The three datasets tend to illustrate the same characteristics in a typical year: maximum upwelling in April and, with the exception of the southernmost coastal winds, a secondary maximum in August-September. The main differences are (1) that the PFEL indices peak later (May-June), (2) that the late summer-fall maxima is of similar (or even larger) magnitude than the spring maxima for the offshore QuikSCAT stations, and (3) that QuikSCAT shows a third maximum in December. The PFEL series at 33°N stands out from the rest, having the strongest annual cycle and the maximum values of upwelling of all. At this latitude, we find the lowest coherences and correlations between the PFEL series and meteorological and QuikSCAT time series.

The above results draw attention to the PFEL indices at 33°N. The spatial wind pattern suggests weak offshore Ekman transport near the shore of the U.S.-México border, increasing steadily towards Punta Baja in the Baja California Peninsula (fig. 2). Sea surface temperature satellite images support the idea of reduced upwelling on the southernmost California coastal region: the monthly composites for March-June (1999–2004) rarely show the presence of cold upwelled waters near the coast between Los Angeles and San Diego, while south of Ensenada (32°N) cold upwelled waters are always present (not shown, see http://coastwatch.pfel.noaa.gov/sst_comp_low.html). This pattern is also observed in the sea surface temperatures taken by the CalCOFI cruises, which in spring and summer show maximum temperatures along the coast in the southern part of the Southern California Bight (Winant and Dorman 1997). By contrast, the satellite images and the CalCOFI data generally show cold waters extending southeastwards of Point Conception, and along the northern coast of the Southern California Bight.

Contrary to this, a 50-year analysis of the PFEL indices along the North America West Coast (21°N–60°N) found the upwelling maximum at 33°N (Schwing et al. 1996). We think this discrepancy is partially due to the position of the PFEL grid point, which is closer to the offshore maximum downstream of Point Conception than it is to the eastern coastline, resulting in an overestimation of the coastal upwelling driven by offshore Ekman transport. But this does not explain why the seasonal variations, the timing and magnitude of maximum upwelling, and the variability of the PFEL indices at 33°N are significantly different compared to all the other time series, including QuikSCAT at that location.

Finally, we join others in cautioning biological oceanographers and marine ecologists on the use of PFEL indices. These indices vary at large spatial scales (>100 km), and they do not capture the small-scale patchiness that is pervasive in marine ecological systems or the high-frequency physical processes that are common in nearshore environments. Use of these indices as independent variables explaining ecological-system response poses problems, as the processes the indices try to capture, such as primary productivity and offshore larval drift, are complex, and often determined by unresolved biological and physical processes. For example, nearshore larvae may not drift offshore in response to suspected upwelling detected by PFEL indices because (1) the indices do not capture accurately the nearshore winds (e.g. this contribution for 33°N), (2) larvae may not be transported offshore by upwelling flows (i.e., they may be transported along-shore, not transported at all, or transported onshore, depending on larval vertical and cross-shore distribution), (3) flows by unaccounted small-scale transport processes dominate larval transport, or simply because (4) there are no larvae to be transported offshore. Hence, larval transport and dispersal of invertebrate and fish larvae are unlikely to be captured by PFEL indices or other large-scale descriptors such as satellite imagery. Before using PFEL indices and large scale

descriptors as independent variables to explain processes such as primary production, fish biomass or intertidal community dynamics, researchers should resolve observationally the relevant biological and physical processes. Use of these indices without observational knowledge of the pelagic processes influencing the biological variables risks perpetuating unsupported hypotheses.

We conclude that the daily PFEL indices at 33°N do not seem representative of the offshore Ekman transport in the coastal region between Los Angeles and San Diego, and that caution should be taken when correlating them with events in the eastern Southern California Bight. On the other hand, the three databases compare reasonably well in Punta Banda and southwards. The QuikSCAT winds in the grid points closest to shore have large RMS errors in direction when compared to the meteorological wind data, but show similar properties of the variance ellipses and have reasonable coherences for frequencies in the weather band and lower, particularly south of 33°N.

ACKNOWLEDGMENTS

We thank Fernando Miranda, Ignacio González, and Sergio Ramos for help in the installation of the meteorological stations, and for recovery and processing of the data. Wind data at La Jolla were provided by the Coastal Data Information Program at Scripps Institution of Oceanography. Modesto Ortíz offered much appreciated advice for the vector time series analysis and its interpretation. The kind comments from two anonymous reviewers helped improve the presentation of this study. This project was partially funded by the U.S. National Science Foundation through grants to J. P. and M. L.

LITERATURE CITED

Ainley, D. G., W. J. Sydeman, R. H. Parrish, and W. H. Lenarz. 1993. Oceanic Factors Influencing Distribution of Young Rockfish (*Sebastes*) in Central California: A Predator's Perspective. Calif. Coop. Oceanic Fish. Invest. Rep., 34:133–139.

Bakun, A. 1975. Daily and weekly upwelling indices, West Coast of North America, 1967–73. U.S. Dep. Commer., NOAA Tech. Rep., NMFS SSRF-693, 114 p.

Bakun, A., and C. S. Nelson. 1977. Climatology of upwelling related processes off Baja California. Calif. Coop. Oceanic Fish. Invest. Rep. 19:107–127.

Bakun, A., and C. S. Nelson. 1991. The Seasonal Cycle of Wind-Stress Curl in Subtropical Eastern Boundary Current Regions. J. Phys. Oceanog. 21(12):1815-1834.

Beardsley, R. C., C. E. Dorman, C. A. Friehe, L. K. Rosenfeld, and C. D. Winant. 1987. Local atmospheric forcing during the Coastal Ocean Dynamics Experiment 1. A description of the marine boundary layer and atmospheric conditions over a northern California upwelling region. J. Geophys. Res. 92:1467–1488.

Capet, X. J., P. Marchesiello, and J. C. McWilliams. 2004. Upwelling response to coastal wind profiles. Geophys. Res. Lett. 31, L13311, doi: 10.1029/2004GL020123.

Connolly, S. R., B. A. Menge, and J. Roughgarden. 2001. A latitudinal gradient in recruitment of intertidal invertebrates in the northeast Pacific Ocean. Ecology. 82:1799–1813.

Emery, W. J, and R. E. Thomson. 2001. Data Analysis Methods in Physical Oceanography. 2nd ed. Netherlands: Elsevier Science B.V. 638 pp.

Enriquez, A. G., and C. A. Friehe. 1995. Effects of Wind Stress and Wind Stress Curl Variability on Coastal Upwelling. J. Phys. Oceanog. 25:1651–1671.

Gonella, J. 1972. A rotary-component method for analyzing meteorological and oceanographic vector time series. Deep-Sea. Res. 19:833–846.

Huyer, A. 1983. Coastal Upwelling in the California Current System. Prog. Oceanog. 12:259–284.

Julian, P. R. Comments on the determination of significance levels of the coherence statistic. J. Atmos. Sci. 32:836–837.

Koracin, D., C. E. Dorman, E. P. Dever. 2004. Coastal Perturbations of Marine-Layer Winds, Wind Stress, and Wind Stress Curl along California and Baja California in June 1999. J. Phys. Oceanog. 34:1152–1173.

Koslow, J. A., A. J. Hobday, and G. W. Boehlert. 2002. Climate variability and marine survival of coho salmon (*Oncorhynchus kisutch*) in the Oregon production area. Fish. Oceanogr. 11:65–77.

Ladah, L. B., and J. A. Zertuche. 2004. Giant kelp (*Macrocystis pyrifera*) survival in deep water (25–40 m) during El Niño of 1997–1998 in Baja California, Mexico. Botanica Marina. 47:367–372.

Longhurst, A. R. 1998. Ecological geography of the sea. 1st ed. London: Academic Press. 398 pp.

Lynn, R. 1967. Seasonal variation of temperature and salinity at 10 meters in the California Current. Calif. Coop. Oceanic Fish. Invest. Rep. 11:157–186.

Mooers, C. N. K. 1973. A technique for the cross spectrum analysis of pairs of complex-valued time series, with emphasis on properties of polarized components and rotational invariants. Deep-Sea Res. 20:1129–1141.

Münchow, A. 2000. Wind stress curl forcing of the coastal ocean near Point Conception, California. J. Phys. Oceanog. 30:1265–1280.

Nelson, C. S. 1977. Wind stress and wind-stress curl over the California Current. NOAA Tech. Rep. NMFS SSRF-714, 87 pp.

Parrish, R. H., and D. L. Mallicoate. 1995. Variation in the condition factors of California pelagic fishes and associated environmental factors. Fish. Oceanogr. 4:171-190.

Peterson, W. T., C. B. Miller, and A. Hutchinson. 1979. Zonation and maintenance of copepod populations in the Oregon upwelling zone. Deep-Sea Res. 26A:467–494.

Pickett, M. H., and J. D. Paduan, 2003. Ekman transport and pumping in the California Current based on the U.S. Navy's high-resolution atmospheric model (COAMPS). J. Geophys. Res. 108(C10), 3327, doi:10.1029/2003JC001902.

Pickett, M. H., W. Tang, L. K. Rosenfeld, and C. H. Wash. 2003. QuikSCAT satellite comparisons with nearshore buoy wind data off the U.S. west coast. J. Atmos. Oceanic Technol. 20:1869–1879.

Pickett, M. H., and F. B. Schwing. 2006. Evaluating upwelling estimates off the west coasts of North and South America. Fish. Oceanogr. 15:256–269.

Rau, G. H., S. Ralston, J. R. Southon, and F. P. Chavez. 2001. Upwelling and the Condition and Diet of Juvenile Rockfish: A Study Using Natural Abundances. Limnol. Oceanog. 46:1565–1570.

Reid, J. L., G. I . Roden, and J. G. Wyllie. 1958. Studies of the California Current system. Calif. Coop. Oceanic Fish. Invest. Rep. 1 July 1956–1 Jan. 1958:27–57.

Roughgarden, J., S. Gaines, and H. Possingham. 1988. Recruitment dynamics in complex life cycles. Science (Washington D.C.) 241:1460–1466.

Ryther, J. H. 1969. Photosynthesis and fish production in the sea. Science (Washington D.C.) 166:72–76.

Schwing, F. B., M. O'Farrell, J. Steger, J., and K. Baltz. 1996: Coastal Upwelling Indices, West Coast of North America 1946–1995, U.S. Dep. Comer., NOAA Tech. Memo., NOAA-TM-NMFS-SWFSC-231, 207 pp.

Strub, P. T., and C. James. 2000. Altimeter-derived variability of surface velocities in the California Current System: 2. Seasonal circulation and eddy statistics. Deep-Sea Res. II, 47:831–870.

Tang, W., W. T. Liu, and B. W. Stillos. 2004. Evaluation of high-resolution ocean surface vector winds measured by QuikSCAT scatterometer in the coastal region. Geosciences and Remote Sensing, IEEE Transactions, 42(8):1762–1769. DOI 10.1109/TGRS.2004.831685.

Winant, C. D., C. E. Dorman, C. A. Friehe, and R. C. Beardsley (1988). The marine layer off northern California: an example of supercritical channel flow. J. Atmos. Sci. 45:3588–3605.

Winant, C. D., and C. E. Dorman, 1997. Seasonal patterns of surface wind stress and heat flux over the Southern California Bight. J. Geophys. Res. 102:5641–5653.